Earth's Future

RESEARCH ARTICLE
10.1029/2020EF001893

Seesaw Terrestrial Wetting and Drying Between Eastern and Western Australia

Ajiao Chen[1], **Huade Guan**[1], **and Okke Batelaan**[1]

[1]National Centre for Groundwater Research and Training, College of Science and Engineering, Flinders University, Adelaide, SA, Australia

Key Points:

- A seesaw wetting/drying phenomenon between eastern and western Australia is revealed for the first time
- This terrestrial water storage (TWS) seesaw pattern is reset by strong La Niña induced continent-wide wetting
- The TWS seesaws appear to be resulting from vegetation mediated hydrological responses to decadal precipitation variability

Supporting Information:

Supporting Information may be found in the online version of this article.

Correspondence to:

H. Guan,
huade.guan@flinders.edu.au

Citation:

Chen, A., Guan, H., & Batelaan, O. (2021). Seesaw terrestrial wetting and drying between eastern and western Australia. *Earth's Future*, *9*, e2020EF001893. https://doi.org/10.1029/2020EF001893

Received 5 NOV 2020
Accepted 19 APR 2021

Abstract Australia, the driest inhabited continent, is prone to natural disasters, such as droughts, floods, bushfires, and heatwaves. Strong climate variability causes recurring threats to water supply, agriculture, and the environment. Improving our insight into changes in hydroclimatic patterns is required to provide useful information for society. Previous studies mainly focused on the causes of extreme wet or dry events in specific periods and their impacts on agriculture and ecosystems. An understanding of long-term spatio-temporal patterns of wetting and drying in Australia is still lacking. Here we show, based on analyses of Gravity Recovery and Climate Experiment satellite derived terrestrial water storage and extended datasets, that there are four consecutive periods of seesaw wetting and drying between eastern and western Australia in the past five decades. The seesaw phenomenon is characterized by eastern Australia gaining water, while western Australia is losing water, and vice versa. Strong La Niña induced continent-wide wetting, resets this pattern, leaving each seesaw to last for 11 $\pm$ 5 years. We provide one possible mechanism related to vegetation response to climate variability and its feedback on hydrological processes to explain the seesaw pattern. The identified recurring seesaw pattern indicates that society would need to become more adaptive in managing forest, water, and disaster risks in the wake of a next strong La Niña induced continent-wide wetting in Australia.

Plain Language Summary Here, we report for the first time a vegetation mediated seesaw wetting/drying phenomenon between eastern and western Australia. The seesaw phenomenon is characterized by eastern Australia gaining water, while western Australia is losing water, and vice versa. It is reset by strong La Niña induced continent-wide wetting. The seesaw phase seems to depend on vegetation cover anomaly prior to the strong La Niña event, and can be explained by subsequent vegetation and soil moisture interactions. This finding provides society with valuable reference for managing forest, water, and disaster risks in the wake of a next strong La Niña induced continent-wide wetting in Australia.

1. Introduction

Australia is the driest inhabited continent on Earth and among the areas of the most variable rainfall in the world (Dey et al., 2019; Nicholls et al., 1997). Its hydroclimatic variations play an important role in the global carbon and water cycles (Ahlström et al., 2015; Xie et al., 2016), occurrence of natural hazards (Johnson et al., 2016; Kiem et al., 2016), and agricultural productivity (Ma et al., 2015). Droughts occurring in Australia during 2000–2009 were reported to have reduced global terrestrial net primary production (Zhao & Running, 2010). Poulter et al. (2014) indicated that the global land carbon sink anomaly triggered by the 2010–2011 La Niña event was largely due to an enhanced ecosystem productivity across the Southern Hemisphere, particularly in Australia. Frequent droughts cause agricultural losses (Heberger, 2012; Van Dijk et al., 2013), contribute to bushfires (Sharples et al., 2016) and exacerbate heatwaves (Herold et al., 2016; Perkins-Kirkpatrick et al., 2016), and consequently impact the economy and society significantly (Van Dijk et al., 2013). This continent is also prone to floods, which lead to serious casualties and economic losses (Johnson et al., 2016). Hence, furthering our understanding and monitoring of wet and dry conditions in Australia is urgently needed for water, agriculture, and disaster risk management.

Previous studies mainly focused on the causes of droughts or floods in discrete periods and their impacts on ecosystems and society (Johnson et al., 2016; Kiem & Verdon-Kidd, 2010; Kiem et al., 2016; Nicholls, 2011; Van Dijk et al., 2013). Hydroclimatic extremes in Australia are usually attributed to the combined effect

of large-scale climate modes such as El Niño Southern Oscillation (ENSO), Indian Ocean Dipole (IOD), and Inter-decadal Pacific Oscillation (IPO) (e.g., King et al., 2020; Ummenhofer et al., 2009; Verdon-Kidd & Kiem, 2009a, 2009b, 2014). The indices of these climate oscillation systems are reported to have strong correlation with rainfall/streamflow in Australia (Cai et al., 2011; Franks, 2004; Kiem et al., 2003; Power et al., 2006). El Niño (La Niña) tends to increase the possibility of dry (wet) conditions across many parts of Australia (Nicholls, 1992; Power et al., 2006; Risbey et al., 2009). For example, an abnormal wet period in 2010–2011 was reportedly driven by one of the strongest La Niña events in the past nine decades (Christidis et al., 2013; Evans & Boyer-Souchet, 2012; King et al., 2013; Nicholls, 2011; Trenberth, 2012). Xie et al. (2016) recently investigated the wet and dry evolution across continental Australia based on Gravity Recovery and Climate Experiment (GRACE) terrestrial water storage (TWS) data set (2002–2014). They revealed three geographic zones with distinct TWS responses and attributed them to different large-scale teleconnections. If such regional differentiated TWS responses hold over a long period, it would provide society useful information for climate-adaptive water resource planning and management. In this study, we aim to reveal long-term spatio-temporal patterns of TWS in Australia, and to examine how these patterns are associated with climate variability and land surface processes.

2. Materials and Methods

2.1. Datasets

2.1.1. TWS Data

Three TWS datasets are used in this study. The first is the original GRACE TWS data set (RL06M.MSCNv01) (Watkins et al., 2015; Wiese et al., 2016) from 2003 to 2016 provided by the NASA Jet Propulsion Laboratory (JPL). Seventeen months of missing TWS data (June 2003, January 2011, June 2011, May 2012, October 2012, March 2013, August 2013, September 2013, February 2014, July 2014, December 2014, June 2015, October 2015, November 2015, April 2016, September 2016, and October 2016) are filled by linear interpolation using the months either side (Andrew et al., 2017; Long et al., 2015). In order to investigate the wetting and drying cycles over a long period, two reconstructed GRACE TWS datasets for 1985–2015 (Humphrey et al., 2017) and for 1901–2014 (Humphrey & Gudmundsson, 2019) are also applied. The TWS data set of 1901–2014 was reconstructed from statistical data-driven models, calibrated with observations, which performs well in comparison with state-of-the-art hydrological models (Humphrey & Gudmundsson, 2019; Padrón et al., 2020). The seasonality of TWS has been removed by subtracting monthly averages, resulting in what is referred to as TWS anomaly in this study. All TWS datasets are of $0.5° \times 0.5°$ spatial resolution.

2.1.2. Normalized Difference Vegetation Index Data

Global Inventory Monitoring and Modeling System (GIMMS) Normalized Difference Vegetation Index (NDVI) data set (Pinzon & Tucker, 2014; Tucker et al., 2005) is available from July 1981 to December 2015. Moderate Resolution Imaging Spectroradiometer (MODIS) NDVI data set (Didan et al., 2015) is available from March 2000. MODIS NDVI data are of $0.5° \times 0.5°$ spatial resolution, and the GIMMS NDVI data were remapped from $1/12° \times 1/12°$ to $0.5° \times 0.5°$ in this study.

2.1.3. Model-Derived Evapotranspiration, Soil Moisture, and Precipitation Data

GLDAS_NOAH025_M evapotranspiration data (Beaudoing & Rodell, 2015; Rodell et al., 2004) are of $0.25° \times 0.25°$ spatial resolution. Soil moisture and precipitation data provided by the Australian Water Availability Project (AWAP) (Raupach et al., 2009, 2018) are of $0.05° \times 0.05°$ spatial resolution.

2.1.4. Ocean-Atmosphere Indices

Two ocean-atmosphere climate indices, the Southern Oscillation Index (SOI) (Allan et al., 1991; Können et al., 1998; Ropelewski & Jones, 1987) and the Indian Ocean Dipole Mode Index (DMI) (Saji, 2003), are applied in this study to examine the role of ENSO and IOD in Australia's hydroclimatic variations (Kiem & Verdon-Kidd, 2010; Van Dijk et al., 2013; Verdon-Kidd & Kiem, 2009a, 2009b).

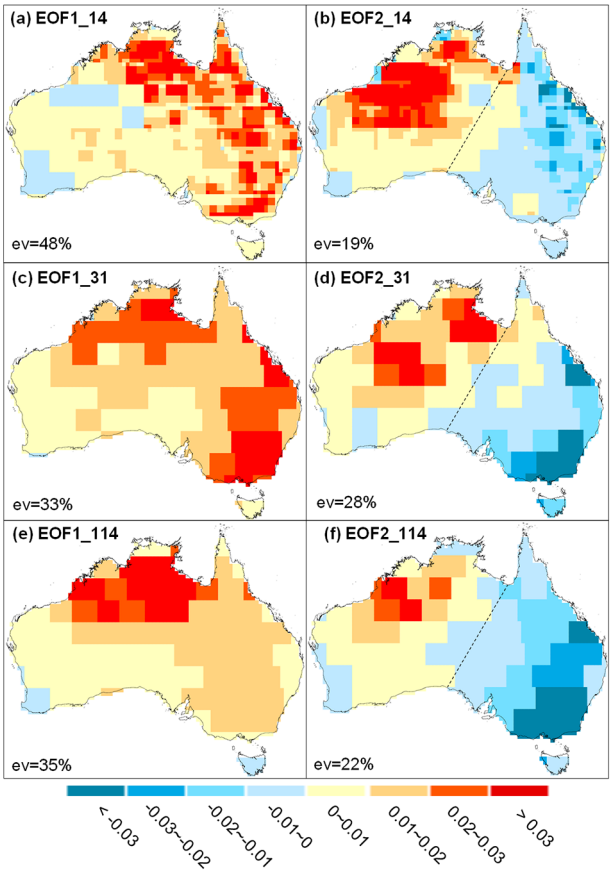

Figure 1. Spatial patterns of the first two modes (EOF1 & EOF2) of Australia TWS variation. (a and b) 14-year original JPL GRACE TWS (2003–2016), (c and d) 31-year reconstructed GRACE TWS (1985–2015), (e and f) 114-year reconstructed GRACE TWS (1901–2014). Acronym "ev" stands for explained variance. An east-west opposite (EOF2) pattern is observed in all three datasets. GRACE, Gravity Recovery and Climate Experiment; JPL, Jet Propulsion Laboratory; TWS, terrestrial water storage.

2.2. Empirical Orthogonal Functions (EOFs)

The EOFs decompose a space-time field into spatial patterns and associated temporal signals. For a continuous space-time field $X(t, s)$, t and s denote respectively time and spatial position, the decomposition is described as in the study of Hannachi et al. (2007):

$$X(t,s) = \sum_{k=1}^{K} c_k(t) u_k(s) \quad (1)$$

where K is the number of modes included in the field, using an optimal set of basis functions of space $u_k(s)$ and expansion functions of time $c_k(t)$. For the space-time field of TWS over Australia, the EOFs method finds a set of orthogonal spatial patterns (EOF_k) along with a set of associated uncorrelated time series or principal components (PC_k) (i.e., PC1 corresponds to EOF1 and so on). This method also provides the explained variance, which indicates how much variability of TWS is explained by each decomposed mode (EOF_k/PC_k).

2.3. Significance Test

The significance of linear trend is tested by the modified Mann-Kendall (M-K) test (Hamed & Ramachandra Rao, 1998). Analysis of covariance is applied to test the significance of difference between two time series. The effective sample size (Bretherton et al., 1999) considering the autocorrelation of datasets is applied in statistical significance testing for the correlation coefficient between two time series. The 0.05 significance level is adopted in this study.

3. Results and Discussion

3.1. Main Spatial Patterns of TWS Variation in Australia

The space-time fields of monthly Australia TWS anomaly from three datasets (14-year original JPL GRACE TWS and reconstructed GRACE TWS of 31 and 114 years) have been decomposed by empirical orthogonal functions (EOFs). We focus on the first two modes since they explain more than 50% of the total variance. The three datasets exhibit similar spatial patterns (Figure 1). Almost all grid cells (more than 90%) show consistent phase in terms of spatial pattern EOF1 (Figures 1a, 1c, and 1e) indicating that the wet and dry alternation has consistency over the whole continent, although the north and east parts have higher variability. This EOF mode explains more than 30% of the total TWS variability in Australia. The spatial pattern EOF2 clearly delineates two zones, eastern and western Australia, with opposite behavior (Figures 1b, 1d, and 1f). This mode is defined as an east-west opposite pattern, which explains around 20% of the total variation of the TWS anomaly in Australia. The dashed line in Figure 1 is drawn based on the average results from the three datasets of different year ranges. This line is coincident with the boundary of the western plateaus and central plains of the Australian continent.

3.2. Four Consecutive Seesaw Wetting and Drying Phases Between Eastern and Western Australia in the Past Five Decades

The temporal signal of the first decomposed mode (PC1) reflects the wet (positive PC1) and dry (negative PC1) conditions in terms of average TWS anomaly over the whole continent. The continent-wide wetting and drying are closely related to large-scale ocean-atmosphere dynamics. As shown in Figure 2, continent-wide wetting episodes represented by positive phases of PC1 generally correspond to positive phases of SOI (La Niña episodes). We use pairs of dashed lines to mark the La Niña induced continent-wide wetting

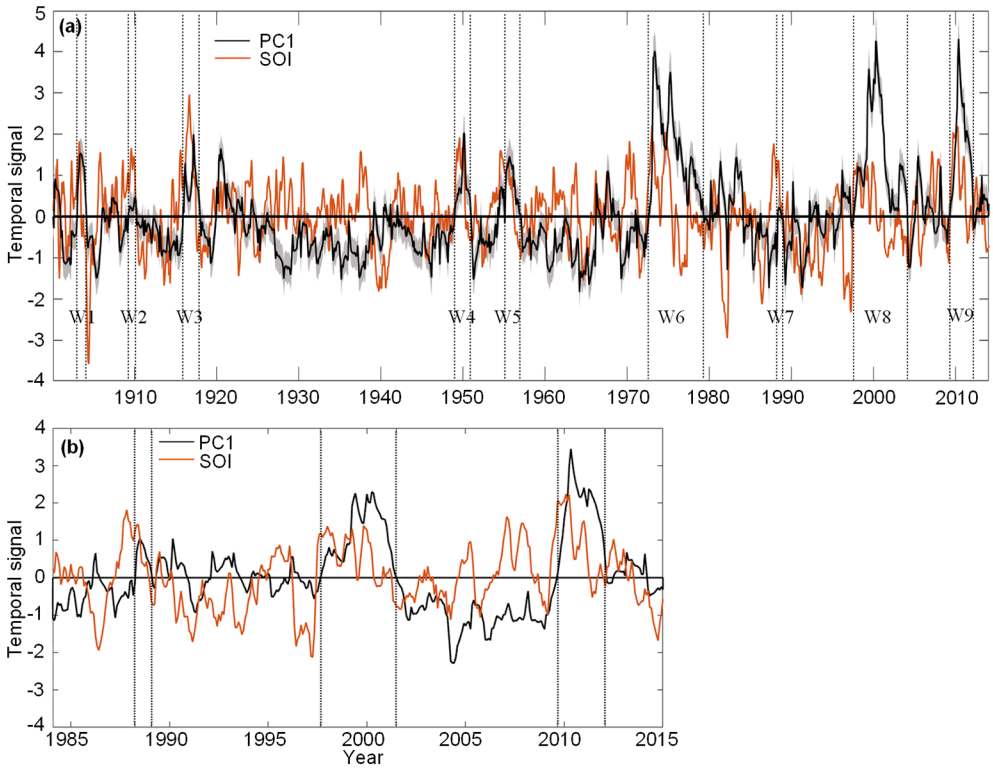

Figure 2. La Niña induced continent-wide wetting episodes identified based on standardized SOI and the temporal signal of the first mode (PC1) of Australia TWS variation. (a) PC1 versus SOI during 1901–2014 ($r = 0.18$, $p < 0.05$). The black curve indicates mean PC1 derived from 100 PC1 members and the shaded areas represent ±1 standard deviation of 100 PC1 time series derived from the ensemble members. A 3-month moving average was applied to SOI for readability (orange curve). The periods marked by a pair of dashed lines (W1–W9) denote the La Niña (positive SOI) induced continent-wide wetting episodes (positive PC1). (b) PC1 versus SOI during 1985–2015 ($r = 0.23$, $p < 0.05$). The three marked La Niña induced continent-wide wetting episodes respectively correspond to W7, W8, and W9 shown in (a). SOI, Southern Oscillation Index; TWS, terrestrial water storage.

episodes, which are bounded by the time points when average TWS anomaly in Australia starts to increase, triggered by strong La Niña, and when it returns to equilibrium. Nine La Niña induced continent-wide wetting episodes are identified during 1901–2014 (W1: December 1903–January 1905, W2: March 1910–February 1911, W3: November 1916–November 1918, W4: December 1949–November 1951, W5: February 1956–December 1957, W6: July 1973–March 1980, W7: April 1989–September 1989, W8: August 1998–June 2002, W9: April 2010–January 2013, see Figure 2a). As this 114-year reconstructed GRACE TWS data set is the mean of 100 ensemble members, uncertainty in PC1 is quantified by ±1 standard deviation of 100 PC1 time series derived from the ensemble members (Figure 2a).

As the eastern and western parts of Australia have opposite phases in EOF2 (Figures 1b, 1d, and 1f), they are supposed to behave oppositely in terms of TWS variation. The periods in-between the La Niña induced continent-wide wetting episodes, show piece-wise linear trends of the regional average TWS anomaly in the eastern and western parts of Australia (Figure 3a). Four consecutive opposite TWS trends between eastern and western Australia are observed during the past five decades (1958–2010). In those four consecutive interval periods, changes of regional average TWS anomaly between the two parts are significantly different at 0.05 significance level (tested by analysis of covariance). This phenomenon is identified as seesaw wetting and drying between these two geographical parts of Australia. The seesaw is characterized by eastern Australia gaining (losing) water, while the west is losing (gaining) water. It appears that a seesaw is reset by a continent-wide wetting episode, leading to a previous gaining (losing)-water side starts to lose (gain) water. Another seesaw phenomenon is observed during the 1910s. These five seesaw periods last for 11 ± 5 years. Uncertainty in regional average TWS time series is represented by the shaded area in Figure 3a. Uncertainty of the consecutive opposite trends in the last four interval periods is quantified in Figure 3b, the average

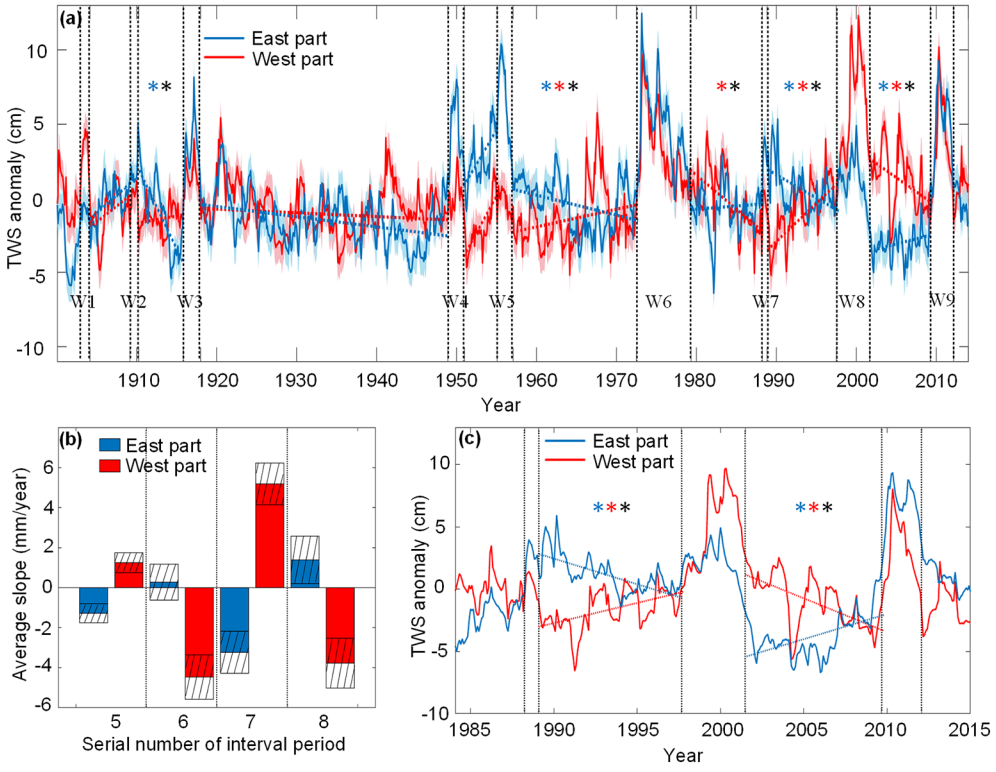

Figure 3. TWS seesaw between eastern and western Australia. (a) Regional average TWS anomaly of eastern and western Australia during 1901–2014 (the boundary of eastern and western parts is shown in Figure 1). Blue (red) asterisk (*) indicates the trend of eastern (western) Australia is significant at 0.05 significance level, and the black asterisk indicates the changes of regional average TWS anomaly between eastern and western Australia are significantly different; (b) slopes of regional average TWS anomaly derived from 100 ensemble members in the last four interval periods (5–8). Hatched bars indicate uncertainty (±1 standard deviation) in trends. (c) Same as (a) but based on TWS data of 1985–2015. TWS, terrestrial water storage.

linear trends of the east and west part derived from 100 ensemble members are significantly different at 0.05 significance level.

The input data for reconstructing the 31- and 114-year TWS include precipitation and temperature information. Data of those two climate variables are of low quality for most of the 114-year time series. Therefore, we repeated above analysis with the 31-year reconstructed TWS data (1985–2015) for comparison. Three La Niña induced continent-wide wetting episodes (April 1989–January 1990, August 1998–June 2002, and August 2010–February 2013) are marked in Figure 2b, which respectively correspond to W7–W9 shown in Figure 2a, although minor differences exist. The regional average TWS anomaly of the eastern and western parts of Australia from 1985 to 2015 are plotted in Figure 3c. Two pairs of opposite trends (all are significant at 0.05 significance level) are observed in the interval periods which correspond to the last two seesaws shown in Figure 3a, respectively.

No seesaw phenomenon is observed if the interval between two La Niña induced continent-wide wetting episodes is too short (1905–1910) or too long (1918–1949). The length of a continent-wide wetting episode (reflected in the PC1 response, Figure 2) and its occurrence frequency are associated with the intensity and duration of the La Niña events, as well as the conjunction effects from other oscillations (e.g., IPO and IOD). From 1918 to 1949, only one moderate La Niña occurred (1938–1939), but it did not induce continent-wide wetting (Figure 2a). This was likely because a positive IPO phase dominated during 1922–1944 (Salinger et al., 2001), which suppressed both the occurrence and magnitude of a La Niña event (Cai & van Rensch, 2012; Folland et al., 2002; Franks, 2004; Gershunov & Barnett, 1998; Guan et al., 2005; Kiem & Franks, 2004; Kiem et al., 2003; King et al., 2013; Power et al., 1999). The wetting episode W7 was short (10 months), which was likely relevant to the positive IPO phase (1978–1998) (Salinger et al., 2001).

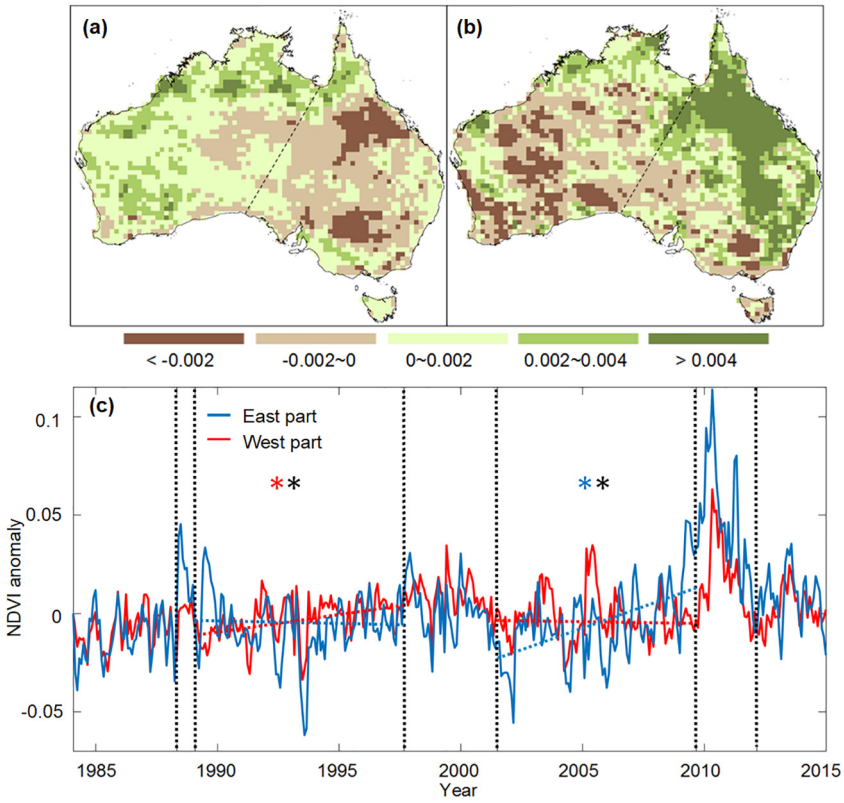

Figure 4. Seesaw phenomenon of NDVI during 1985–2015. (a and b) Linear trends (per month) of NDVI during two interval periods (February 1990–July 1998 and July 2002–July 2010); (c) same as Figure 3c but for NDVI anomaly. NDVI, Normalized Difference Vegetation Index.

Different from the situation in the previous positive IPO (1922–1944), the La Niña in W7 was strong enough to lead to a continent-wide wetting and reset the seesaw between eastern and western Australia. Here, the La Niña coincident with a negative IOD (Figure S1) could explain this situation. Negative IOD usually enhances the La Niña effect, it can also lead to a wetter than normal condition in western and southern Australia (Cai et al., 2014; Risbey et al., 2009).

3.3. Independent Evidence for TWS Seesaw Between Eastern and Western Australia

A soil moisture data set for 1901–2014 (provided by AWAP) also shows a seesaw pattern (Figure S2a) consistent with that of TWS shown in Figure 3a. The agreement between the results based on two independent data sources supports the validity of the TWS seesaw between the two parts of Australia, because changes in soil moisture are typically the largest component of TWS variation (Rodell & Famiglietti, 2001).

In addition, as ecosystems are mostly water limited in Australia, changes of TWS should have led to and be reflected in vegetation responses. GIMMS NDVI data set provides an opportunity to verify the most recent two TWS seesaw phenomena (February 1990–July 1998 and July 2002–July 2010, following the intervals identified based on 31-year reconstructed TWS data). Linear NDVI trends during those two seesaws at each grid cell are shown in Figures 4a and 4b respectively. A marked east-west difference in NDVI trends is observed for both periods. During February 1990–July 1998, NDVI anomaly increases in the western region and decreases in the eastern region of Australia (Figure 4a), which is consistent with TWS wetting in the west and drying in the east (Figure 3c). During July 2002–July 2010, NDVI anomaly (Figure 4b) also shows consistent trends with TWS (Figure 3c). Similar to Figure 3c, we plot the regional average NDVI anomaly of eastern and western Australia from 1985 to 2015 in Figure 4c. During the interval between W7 and W8, the regional average NDVI anomaly significantly increases in the west and slightly decreases in the east. During the interval between W8 and W9, average NDVI anomaly significantly increases in the east and slightly

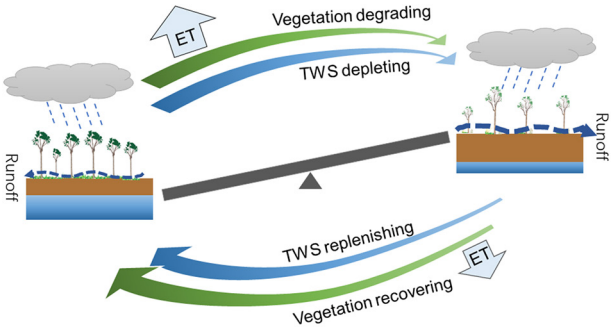

Figure 5. A schematic showing possible TWS and vegetation interactions, leading to TWS seesaw and its resetting by big wetting episodes. TWS, terrestrial water storage.

decreases in the west. Changes of regional average NDVI anomaly between the two parts are significantly different in both interval periods (Figure 4c). These NDVI seesaws, consistent with those of TWS ones, between the western and eastern parts of Australia, provide strong support for the seesaw pattern of TWS variation in Australia.

3.4. Possible Mechanism of the Australia TWS Seesaw Phenomenon

For the four consecutive TWS seesaws between eastern and western Australia, the seesaw state seems to be reset by a continent-wide wetting episode. In other words, if a region was gaining water before the wetting episode, it would be losing water after that. Since TWS is mainly recharged by precipitation, we attempted to explain the seesaw phenomenon of TWS by looking into precipitation patterns. The regional average precipitation (provided by AWAP) in the eastern and western parts of Australia during 1901–2014 is plotted in Figure S2b. Opposite trends between two parts are shown for the last three intervals. After the regional average precipitation time series being smoothed, those three pairs of opposite trends are significantly different in each interval (Figure S2c). It appears that precipitation alone cannot explain the TWS seesaw because in the second (between W2 and W3) and fifth (between W5 and W6) interval periods the seesaw phenomenon is only observed in TWS but not in precipitation.

Here, we provide one possible mechanism related to dynamic woody vegetation and soil moisture interactions, which appears to explain the seesaw resetting pattern (Figure 5). For a region with an increasing TWS (the lower blue arrow in Figure 5) during a seesaw period, vegetation cover tends to be well developed prior to a wetting episode. Such an improved vegetation cover makes the region to have a larger than normal storm water retention capacity for big wetting events, for example, by root enhanced infiltration and organic matter facilitated soil hydrophilicity (Guan et al., 2010; Lange et al., 2009; Wang et al., 2013). Following the wetting episode, this increasing vegetation cover tends to demand more root water uptake, which gradually depletes soil moisture, and thus TWS (the upper blue arrow in Figure 5). This process reverses the previous positive TWS trend to a negative one.

In contrast, for a region with a decreasing TWS (the upper blue arrow in Figure 5) during a seesaw period, vegetation cover will reduce. Such a surface tends to favor runoff generation and soil erosion, leading to a lower storm water retention (Dunjó et al., 2004; Kothyari et al., 2004; Mohammad & Adam, 2010). Since Australia is prone to wildfires, the storm water retention can be further weakened by fire-induced hydrophobic soils (Mataix-Solera et al., 2011). After the wetting episode, the previously reduced vegetation cover demands less soil moisture, leading to a gradual increase of TWS (the lower blue arrow in Figure 5) during the interval period.

The above two situations explain the seesaw resetting pattern in which a positive (negative) seesaw stage is reset to a negative (positive) one after a short wetting episode. This mechanism highlights the important role of vegetation and soil moisture interactions in the observed TWS seesaws. The possibility of this vegetation mediation for the seesaw phenomenon is further supported by comparing spatial patterns of linear trends of relevant variables. The spatial pattern of TWS trends (Figures S3a and S3b) matches better with that of NDVI (Figures 4a and 4b) than that of precipitation (Figures S3c and S3d), suggesting that the vegetation mediation effect is very likely the primary influence on the TWS seesaw phenomenon. The mechanism of vegetation recovering (degrading) illustrated in Figure 5 can be enhanced by in-phase trends of precipitation. For example, in the last three interval periods precipitation shows opposite trends between the eastern and western parts of Australia, which are consistent with those of TWS.

By comparing the 12-month average NDVI anomaly immediately before (Figures 6a–6c) and 12-month average TWS anomaly immediately after (Figures 6d–6f) the three La Niña induced continent-wide wetting episodes shown in Figure 2b, we can see that the half of the continent (either east or west) with increased vegetation cover (positive NDVI anomaly) prior to a La Niña triggered wetting episode, retains larger than normal storm water (positive TWS anomaly) after the episode. After a wetting episode, the part dominated

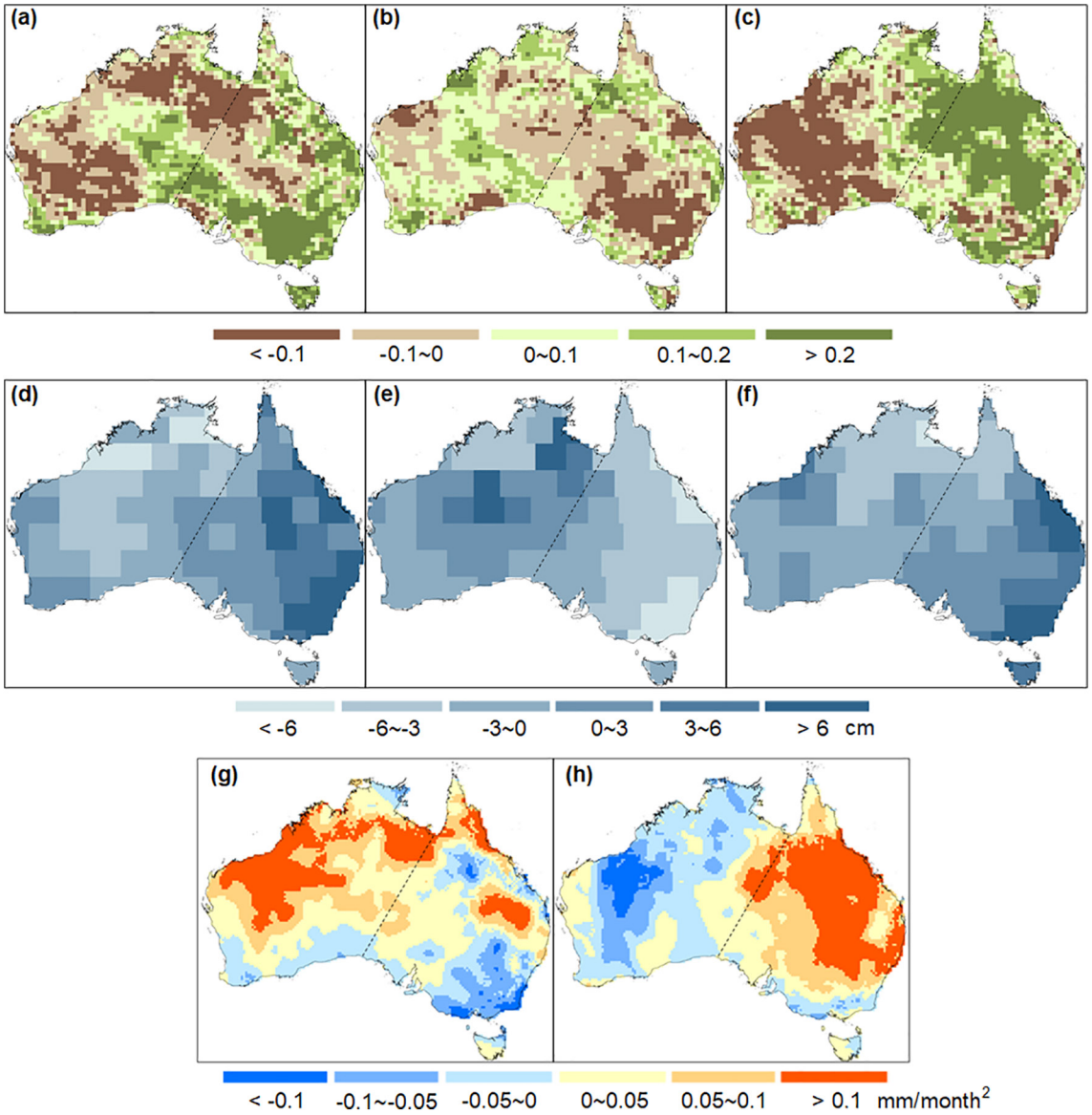

Figure 6. Evidence for the possible mechanism of the TWS seesaw phenomenon. Average 12-month NDVI anomaly (a–c) immediately before and average 12-month TWS anomaly (d–f) immediately after the three continent-wide wetting episodes: April 1989–January 1990, August 1998–June 2002, and August 2010–February 2013; (g and h) linear trends of evapotranspiration (ET) during two interval periods: February 1990–July 1998 and July 2002–July 2010.

by positive NDVI and TWS anomalies experiences a decreasing evapotranspiration (ET) (Figures 6g and 6h), reflecting a gradually decreasing vegetation cover resulting from a depleting TWS. These processes are consistent with the trends of NDVI and TWS during the corresponding interval period. In addition, vegetation in the region with positive (negative) NDVI anomaly prior to the last La Niña induced continent-wide wetting shows a decreasing (increasing) trend during March 2013–December 2018 (Figure S4). Such results support the mechanism of the TWS seesaw phenomenon for Australia, which we explained in Figure 5.

Based on this understanding, we suppose that vegetation dynamic, in response to continent-wide wetting, plays an important role in the TWS seesaw in Australia. However, the interval period should be long enough for woody vegetation to recover in one part while to degrade in the other part of Australia, so that TWS seesaw between the two parts could be reset by a La Niña induced continent-wide wetting.

4. Conclusions

This study, based on three TWS datasets (14-year original JPL GRACE TWS and 31- and 114-year reconstructed GRACE TWS), elucidates a new spatio-temporal pattern of wetting-drying over Australia. Four consecutive seesaw wetting and drying phases between eastern and western Australia are observed in the past five decades, which is characterized by eastern Australia gaining water while the western part is losing water, and vice versa. Strong La Niña induced continent-wide wetting, resets this pattern, leaving each seesaw to last for 11 ± 5 years. The TWS seesaw phenomenon is substantiated by a similar pattern in NDVI between eastern and western Australia during February 1990–July 1998 and July 2002–July 2010. This continental scale TWS seesaw pattern seems to be resulting from woody vegetation response to climate variability and its feedback on hydrological processes.

The results of this study contribute to a better understanding of drying and wetting phases and hence can stimulate an adaptive forest, water, and disaster risk management in the wake of a strong La Niña induced continent-wide wetting in Australia. Our finding suggests that at the end of a seesaw drying phase, poor vegetation cover limits the landscape water retention capacity. Hence, during a drying phase a reasonable management response might be to increase storm water harvesting capacity. At the beginning of a seesaw drying phase, previously increased vegetation cover (resulting from a previous seesaw wetting) depletes root zone moisture, leading to landscape degradation in the subsequent years. Reducing vegetation cover right after the wetting episode might reduce the risk of heatwaves and bushfires in the later dry stage.

Data Availability Statement

The datasets used in this study are available online in the following locations: JPL GRACE TWS, https://grace.jpl.nasa.gov/; reconstructed TWS from 1985 to 2015 (GRACE_REC_v01), http://rossa-prod-ap21.ethz.ch/delivery/DeliveryManagerServlet?dps_pid=IE5766472; reconstructed TWS from 1901 to 2014 (GRACE_REC_v03), https://doi.org/10.6084/m9.figshare.7670849; GIMMS NDVI, https://climatedataguide.ucar.edu/climate-data/ndvi-normalized-difference-vegetation-index-3rd-generation-nasagfsc-gimms; MODIS NDVI, https://neo.sci.gsfc.nasa.gov/view.php?datasetId=MOD_NDVI_M; GLDAS_NOAH ET, https://disc.gsfc.nasa.gov/datasets/GLDAS_NOAH025_M_2.0/summary?keywords=GLDAS; SOI index, https://www.esrl.noaa.gov/psd/gcos_wgsp/Timeseries/SOI/; DMI index, https://www.esrl.noaa.gov/psd/gcos_wgsp/Timeseries/DMI/. AWAP soil moisture and precipitation data are viewable at: http://www.csiro.au/awap and downloadable via ftp by application to Peter.Briggs@csiro.au.

Acknowledgments
We are thankful to the National Aeronautics and Space Administration (NASA), the National Center for Atmospheric Research (NCAR), the National Oceanic and Atmospheric Administration (NOAA), the Institute for Atmospheric and Climate Science, Eidgenössische Technische Hochschule Zurich (IAC, ETH), and the Australian Water Availability Project (AWAP) Team for their provision of data. The first author's PhD scholarship has been provided by the China Scholarship Council, Ministry of Education, China, and Flinders University, Australia. We confirm that all authors have no conflict of interest to declare and agree with the contents.

References

Ahlström, A., Raupach, M. R., Schurgers, G., Smith, B., Arneth, A., Jung, M., et al. (2015). The dominant role of semi-arid ecosystems in the trend and variability of the land CO_2 sink. *Science*, *348*, 895–899. https://doi.org/10.1126/science.aaa1668

Allan, R. J., Nicholls, N., Jones, P. D., & Butterworth, I. J. (1991). A further extension of the Tahiti-Darwin SOI, early ENSO events and Darwin pressure. *Journal of Climate*, *4*, 743–749. https://doi.org/10.1175/1520-0442(1991)004<0743:AFEOTT>2.0.CO;2

Andrew, R., Guan, H., & Batelaan, O. (2017). Estimation of GRACE water storage components by temporal decomposition. *Journal of Hydrology*, *552*, 341–350. https://doi.org/10.1016/j.jhydrol.2017.06.016

Beaudoing, H., Rodell, M., & NASA/GSFC/HSL. (2015). *GLDAS Noah Land Surface Model L4 monthly 0.25 × 0.25 degree V2.0, Greenbelt, Maryland, USA, Goddard Earth Sciences Data and Information Services Center (GES DISC)*. https://doi.org/10.5067/9SQ1B3ZXP2C5

Bretherton, C. S., Widmann, M., Dymnikov, V. P., Wallace, J. M., & Bladé, I. (1999). The effective number of spatial degrees of freedom of a time-varying field. *Journal of Climate*, *12*(7), 1990–2009. https://doi.org/10.1175/1520-0442(1999)012<1990:TENOSD>2.0.CO;2

Cai, W., Purich, A., Cowan, T., van Rensch, P., & Weller, E. (2014). Did climate change-induced rainfall trends contribute to the Australian millennium drought? *Journal of Climate*, *27*, 3145–3168. https://doi.org/10.1175/JCLI-D-13-00322.1

Cai, W., & van Rensch, P. (2012). The 2011 southeast Queensland extreme summer rainfall: A confirmation of a negative Pacific Decadal Oscillation phase? *Geophysical Research Letters*, *39*, L08702. https://doi.org/10.1029/2011GL050820

Cai, W., van Rensch, P., Cowan, T., & Hendon, H. H. (2011). Teleconnection pathways of ENSO and the IOD and the mechanisms for impacts on Australian rainfall. *Journal of Climate*, *24*, 3910–3923. https://doi.org/10.1175/2011JCLI4129.1

Christidis, N., Stott, P. A., Karoly, D. J., & Ciavarella, A. (2013). An attribution study of the heavy rainfall over Eastern Australia in March 2012. *Bulletin of the American Meteorological Society*, *94*(9), S58–S61.

Dey, R., Lewis, S. C., Arblaster, J. M. & Abram, N. J. (2019) A review of past and projected changes in Australia's rainfall. *WIREs Climate Change*, *10*, e577. https://doi.org/10.1002/wcc.577

Didan, K., Barreto Munoz, A., Solano, R., & Huete, A. (2015). *MODIS vegetation index users guide*.

Dunjó, G., Pardini, G., & Gispert, M. (2004). The role of land use-land cover on runoff generation and sediment yield at a microplot scale, in a small Mediterranean catchment. *Journal of Arid Environments*, *57*(2), 239–256. https://doi.org/10.1016/S0140-1963(03)00097-1

Evans, J. P., & Boyer-Souchet, I. (2012). Local sea surface temperatures add to extreme precipitation in northeast Australia during La Niña. *Geophysical Research Letters*, *39*, L10803. https://doi.org/10.1029/2012GL052014

Folland, C. K., Renwick, J. A., Salinger, M. J., & Mullan, A. B. (2002). Relative influences of the Interdecadal Pacific Oscillation and ENSO on the South Pacific Convergence Zone. *Geophysical Research Letters*, *29*(13), 1643. https://doi.org/10.1029/2001GL014201

Franks, S. W. (2004). Multi-decadal climate variability, New South Wales, Australia. *Water Science and Technology*, *49*(7), 133–140. https://doi.org/10.2166/wst.2004.0437

Gershunov, A., & Barnett, T. P. (1998). Interdecadal modulation of ENSO teleconnections. *Bulletin of the American Meteorological Society*, *79*, 2715–2725. https://doi.org/10.1175/1520-0477(1998)079<2715:IMOET>2.0.CO;2

Guan, H., Simunek, J., Newman, B. D., & Wilson, J. L. (2010). Modelling investigation of water partitioning at a semiarid ponderosa pine hillslope. *Hydrological Processes*, *24*, 1095–1105. https://doi.org/10.1002/hyp.7571

Guan, H., Vivoni, E. R., & Wilson, J. L. (2005). Effects of atmospheric teleconnections on seasonal precipitation in mountainous regions of the southwestern U.S. A case study in northern New Mexico. *Geophysical Research Letters*, *32*, L23701. https://doi.org/10.1029/2005GL023759

Hamed, K. H., & Ramachandra Rao, A. (1998). A modified Mann-Kendall trend test for autocorrelated data. *Journal of Hydrology*, *204*, 182–196. https://doi.org/10.1016/s0022-1694(97)00125-x

Hannachi, A., Jolliffe, I. T., & Stephenson, D. B. (2007). Empirical orthogonal functions and related techniques in atmospheric science: A review. *International Journal of Climatology*, *27*(9), 1119–1152. https://doi.org/10.1002/joc.1499

Heberger, M. (2012). Australia's Millennium Drought: Impacts and responses. In P. H. Gleick (Ed.), *The World's Water* (pp. 97–125). Island Press. https://doi.org/10.5822/978-1-59726-228-6_5

Herold, N., Kala, J., & Alexander, L. V. (2016). The influence of soil moisture deficits on Australian heatwaves. *Environmental Research Letters*, *11*, 064003. https://doi.org/10.1088/1748-9326/11/6/064003

Humphrey, V., & Gudmundsson, L. (2019). GRACE-REC: a reconstruction of climate-driven water storage changes over the last century. *Earth System Science Data*, *11*(3), 1153–1170. https://doi.org/10.5194/essd-11-1153-2019

Humphrey, V., Gudmundsson, L., & Seneviratne, S. I. (2017). A global reconstruction of climate-driven subdecadal water storage variability. *Geophysical Research Letters*, *44*, 2300–2309. https://doi.org/10.1002/2017GL072564

Johnson, F., White, C. J., van Dijk, A., Ekstrom, M., Evans, J. P., Jakob, D., et al. (2016). Natural hazards in Australia: floods. *Climatic Change*, *139*, 21–35. https://doi.org/10.1007/s10584-016-1689-y

Kiem, A. S., & Franks, S. W. (2004). Multi-decadal variability of drought risk, eastern Australia. *Hydrological Processes*, *18*(11), 2039–2050. https://doi.org/10.1002/hyp.1460

Kiem, A. S., Franks, S. W., & Kuczera, G. (2003). Multi-decadal variability of flood risk. *Geophysical Research Letters*, *30*(2), 1035. https://doi.org/10.1029/2002GL015992

Kiem, A. S., Johnson, F., Westra, S., Van Dijk, A., Evans, J. P., O'Donnell, A., et al. (2016). Natural hazards in Australia: droughts. *Climatic Change*, *139*, 37–54. https://doi.org/10.1007/s10584-016-1798-7

Kiem, A. S., & Verdon-Kidd, D. C. (2010). Towards understanding hydroclimatic change in Victoria, Australia - preliminary insights into the "Big Dry". *Hydrology and Earth System Sciences*, *14*, 433–445. https://doi.org/10.5194/hess-14-433-2010

King, A. D., Alexander, L. V., & Donat, M. G. (2013). Asymmetry in the response of eastern Australia extreme rainfall to low-frequency Pacific variability. *Geophysical Research Letters*, *40*(10), 2271–2277. https://doi.org/10.1002/grl.50427

King, A. D., Lewis, S. C., Perkins, S. E., Alexander, L. V., Donat, M. G., Karoly, D. J., & Black, M. T. (2013). Limited evidence of anthropogenic influence on the 2011-12 Extreme Rainfall over Southeast Australia. *Bulletin of the American Meteorological Society*, *94*(9): S55–S58.

King, A. D., Pitman, A. J., Henley, B. J., Ukkola, A. M., & Brown, J. R. (2020). The role of climate variability in Australian drought. *Nature Climate Change*, *10*, 177–179. https://doi.org/10.1038/s41558-020-0718-z

Können, G. P., Jones, P. D., Kaltofen, M. H., & Allan, R. J. (1998). Pre-1866 extensions of the Southern Oscillation Index using early Indonesian and Tahitian meteorological readings. *Journal of Climate*, *11*, 2325–2339. https://doi.org/10.1175/1520-0442(1998)011<2325:PEOTSO>2.0.CO;2

Kothyari, B. P., Verma, P. K., Joshi, B. K., & Kothyari, U. C. (2004). Rainfall-runoff-soil and nutrient loss relationships for plot size areas of bhetagad watershed in Central Himalaya, India. *Journal of Hydrology*, *293*(1-4), 137–150. https://doi.org/10.1016/j.jhydrol.2004.01.011

Lange, B., Lüescher, P., & Germann, P. F. (2009). Significance of tree roots for preferential infiltration in stagnic soils. *Hydrology and Earth System Sciences*, *13*, 1809–1821. https://doi.org/10.5194/hess-13-1809-2009

Long, D., Yang, Y., Wada, Y., Hong, Y., Liang, W., Chen, Y., et al. (2015). Deriving scaling factors using a global hydrological model to restore GRACE total water storage changes for China's Yangtze River Basin. *Remote Sensing of Environment*, *168*, 177–193. https://doi.org/10.1016/j.rse.2015.07.003

Ma, X., Huete, A., Moran, S., Ponce-Campos, G., & Eamus, D. (2015). Abrupt shifts in phenology and vegetation productivity under climate extremes. *Journal of Geophysical Research: Biogeosciences*, *120*, 2036–2052. https://doi.org/10.1002/2015JG003144

Mataix-Solera, J., Cerdà, A., Arcenegui, V., Jordán, A., & Zavala, L. M. (2011). Fire effects on soil aggregation: A review. *Earth-Science Reviews*, *109*(1-2), 44–60. https://doi.org/10.1016/j.earscirev.2011.08.002

Mohammad, A. G., & Adam, M. A. (2010). The impact of vegetative cover type on runoff and soil erosion under different land uses. *Catena*, *81*(2), 97–103. https://doi.org/10.1016/j.catena.2010.01.008

Nicholls, N. (1992). Historical El Niño/Southern oscillation variability in the Australian region. In H. F. Diaz, & V. Markgraf (Eds.), *El Nino, historical and paleoclimatic aspects of the southern oscillation* (pp. 151–174). Cambridge Academic Press.

Nicholls, N. (2011). What caused the eastern Australia heavy rains and floods of 2010/11. *Bulletin of the Australian Meteorological and Oceanographic Society*, *24*, 33–34.

Nicholls, N., Drosdowsky, W., & Lavery, B. (1997). Australian rainfall variability and change. *Weather*, *52*, 66–72. https://doi.org/10.1002/j.1477-8696.1997.tb06274.x

Padrón, R. S., Gudmundsson, L., Decharme, B., Ducharne, A., Lawrence, D. M., Mao, J., et al. (2020). Observed changes in dry-season water availability attributed to human-induced climate change. *Nature Geoscience*, *13*, 477–481. https://doi.org/10.1038/s41561-020-0594-1

Perkins-Kirkpatrick, S. E., White, C. J., Alexander, L. V., Argüeso, D., Boschat, G., Cowan, T., et al. (2016). Natural hazards in Australia: Heatwaves. *Climatic Change*, *139*, 101–114. https://doi.org/10.1007/s10584-016-1650-0

Pinzon, J., & Tucker, C. (2014). A Non-Stationary 1981-2012 AVHRR NDVI3g Time Series. *Remote Sensing*, *6*, 6929–6960. https://doi.org/10.3390/rs6086929

Poulter, B., Frank, D., Ciais, P., Myneni, R. B., Andela, N., Bi, J., et al. (2014). Contribution of semi-arid ecosystems to interannual variability of the global carbon cycle. *Nature*, *509*, 600–603. https://doi.org/10.1038/nature13376

Power, S., Casey, T., Folland, C., Colman, A., & Mehta, V. (1999). Inter-decadal modulation of the impact of ENSO on Australia. *Climate Dynamics*, *15*, 319–324. https://doi.org/10.1007/s003820050284

Power, S., Haylock, M., Colman, R., & Wang, X. (2006). The predictability of interdecadal changes in ENSO activity and ENSO teleconnections. *Journal of Climate*, *19*, 4755–4771. https://doi.org/10.1175/JCLI3868.1

Raupach, M. R., Briggs, P. R., Haverd, V., King, E. A., Paget, M. & Trudinger, C. M. (2009). *Australian Water Availability Project (AWAP): CSIRO Marine and Atmospheric Research Component: Final Report for Phase 3*. CAWCR Technical Report No. 013. p. 67.

Raupach, M. R., Briggs, P. R., Haverd, V., King, E. A., Paget, M., & Trudinger, C. M. (2018). *Australian Water Availability Project, Data Release 26m*. CSIRO Oceans and Atmosphere.

Risbey, J. S., Pook, M. J., McIntosh, P. C., Wheeler, M. C., & Hendon, H. H. (2009). On the remote drivers of rainfall variability in Australia. *Monthly Weather Review*, *137*, 3233–3253. https://doi.org/10.1175/2009MWR2861.1

Rodell, M., & Famiglietti, J. S. (2001). An analysis of terrestrial water storage variations in Illinois with implications for the Gravity Recovery and Climate Experiment (GRACE). *Water Resources Research*, *37*(5), 1327–1339. https://doi.org/10.1029/2000WR900306

Rodell, M., Houser, P. R., Jambor, U., Gottschalck, J., Mitchell, K., Meng, C.-J., et al. (2004). The global land data assimilation system. *Bulletin of the American Meteorological Society*, *85*, 381–394. https://doi.org/10.1175/BAMS-85-3-381

Ropelewski, C. F., & Jones, P. D. (1987). An extension of the Tahiti-Darwin Southern Oscillation Index. *Monthly Weather Review*, *115*, 2161–2165. https://doi.org/10.1175/1520-0493(1987)115<2161:AEOTTS>2.0.CO;2

Saji, N., & Yamagata, T. (2003). Possible impacts of Indian Ocean Dipole mode events on global climate. *Climate Research*, *25*(2), 151–169. https://doi.org/10.3354/cr025151

Salinger, M. J., Renwick, J. A., & Mullan, A. B. (2001). Interdecadal Pacific Oscillation and South Pacific climate. *International Journal of Climatology*, *21*, 1705–1721. https://doi.org/10.1002/joc.691

Sharples, J. J., Cary, G. J., Fox-Hughes, P., Mooney, S., Evans, J. P., Fletcher, M.-S., et al. (2016). Natural hazards in Australia: Extreme bushfire. *Climatic Change*, *139*, 85–99. https://doi.org/10.1007/s10584-016-1811-1

Trenberth, K. E. (2012). Framing the way to relate climate extremes to climate change. *Climatic Change*, *115*, 283–290. https://doi.org/10.1007/s10584-012-0441-5

Tucker, C. J., Pinzon, J. E., Brown, M. E., Slayback, D. A., Pak, E. W., Mahoney, R., et al. (2005). An extended AVHRR 8-km NDVI dataset compatible with MODIS and SPOT vegetation NDVI data. *International Journal of Remote Sensing*, *26*, 4485–4498. https://doi.org/10.1080/01431160500168686

Ummenhofer, C. C., England, M. H., McIntosh, P. C., Meyers, G. A., Pook, M. J., Risbey, J. S., et al. (2009). What causes southeast Australia's worst droughts? *Geophysical Research Letters*, *36*, L04706. https://doi.org/10.1029/2008GL036801

Van Dijk, A. I. J. M., Beck, H. E., Crosbie, R. S., de Jeu, R. A. M., Liu, Y. Y., Podger, G. M., et al. (2013). The Millennium Drought in southeast Australia (2001-2009): Natural and human causes and implications for water resources, ecosystems, economy, and society. *Water Resources Research*, *49*, 1040–1057. https://doi.org/10.1002/wrcr.20123

Verdon-Kidd, D. C., & Kiem, A. S. (2009a). Nature and causes of protracted droughts in southeast Australia: Comparison between the Federation, WWII, and Big Dry droughts. *Geophysical Research Letters*, *36*, L22707. https://doi.org/10.1029/2009GL041067

Verdon-Kidd, D. C., & Kiem, A. S. (2009b). On the relationship between large-scale climate modes and regional synoptic patterns that drive Victorian rainfall. *Hydrology and Earth System Sciences*, *13*(4), 467–479. https://doi.org/10.5194/hess-13-467-2009

Verdon-Kidd, D. C., & Kiem, A. S. (2014). Synchronicity of historical dry spells in the Southern Hemisphere. *Hydrology and Earth System Sciences*, *18*, 2257–2264. https://doi.org/10.5194/hess-18-2257-2014

Wang, C., Zhao, C., Xu, Z., Wang, Y., & Peng, H. (2013). Effect of vegetation on soil water retention and storage in a semi-arid alpine forest catchment. *Journal of Arid Land*, *5*, 207–219. https://doi.org/10.1007/s40333-013-0151-5

Watkins, M. M., Wiese, D. N., Yuan, D.-N., Boening, C., & Landerer, F. W. (2015). Improved methods for observing Earth's time variable mass distribution with GRACE using spherical cap mascons. *Journal of Geophysical Research: Solid Earth*, *120*, 2648–2671. https://doi.org/10.1002/2014JB011547

Wiese, D. N., Landerer, F. W., & Watkins, M. M. (2016). Quantifying and reducing leakage errors in the JPL RL05M GRACE mascon solution. *Water Resources Research*, *52*, 7490–7502. https://doi.org/10.1002/2014JB01154710.1002/2016wr019344

Xie, Z., Huete, A., Restrepo-Coupe, N., Ma, X., Devadas, R., & Caprarelli, G. (2016). Spatial partitioning and temporal evolution of Australia's total water storage under extreme hydroclimatic impacts. *Remote Sensing of Environment*, *183*, 43–52. https://doi.org/10.1016/j.rse.2016.05.017

Zhao, M., & Running, S. W. (2010). Drought-induced reduction in global terrestrial net primary production from 2000 through 2009. *Science*, *329*, 940–943. https://doi.org/10.1126/science.1192666